

The Dependence of Electrochemical Behaviors on the Corrosion Products of L360NCS Steel Exposed to Wet H₂S Environments

Liqiang Chen, Jie Zhou, Yuxin Chen, Pengpeng Bai, Jian Wu, Shuqi Zheng*

Beijing Key Laboratory of Failure, Corrosion and Protection of Oil/gas Facilities and Department of Materials Science and Engineering, China University of Petroleum, Beijing 102249, P R China

*E-mail: zhengsq09@163.com

Received: 10 January 2016 / Accepted: 29 February 2016 / Published: 1 April 2016

The corrosion behavior and electrochemical characteristics of carbon steel in H₂S environment were investigated in this paper under different temperatures. Results showed that the corrosion rate of steel increased first from 0.413 mm/a to 0.889 mm/a with the temperature changed from 25 to 75 °C, and then decreased to 0.298 mm/a with the temperature increased to 90 °C. Electrochemical impedance spectroscopy (EIS) showed that the reaction presented charge-transfer and diffusion-controlled mechanism when temperature ranged from 25 to 75 °C; while at 90 °C, the result showed a charge-transfer reaction. The polarization curve revealed the linear polarization resistance (LPR) decreased first and then increased as temperature rose. The results related to the reduced solubility of H₂S in water and enhanced reaction rate with increased temperature. Mackinawite was the main corrosion product, and the ratio of mackinawite increased while the grain size of corrosion products decreased with the increase of temperature.

Keywords: Carbon steel; Electrochemical impedance spectroscopy (EIS); Oil and gas; Sulfidation; Weight loss

1. INTRODUCTION

In recent decades, with the rapid development of global industrial level, requirement of petroleum and natural gas sustained growing, thus, an increasing number of oil and gas fields containing hydrogen sulfide (H₂S) have been developed [1]. Long distance transportation was required due to the unbalanced distribution of oil and gas resources and their consumer markets [2]. Pipeline transportation became an important means of oil and gas long distance transportation because of its characteristics of low costs and large conveying capacity. However, the application of pipeline steel was limited owing to the corrosion when exposed to H₂S environment.

Corrosion is one of the main forms which threat safety of oil and gas pipeline, it brings about pipeline fracture and it is the root of catastrophic accidents [3]. H₂S corrosion is the most serious corrosion problem in pipeline transportation. H₂S not only causes uniform corrosion, localized corrosion, pitting and failures, but also leads to metal's sudden sulfide stress cracking (SSC) and hydrogen induced cracking (HIC), which bring about huge economic losses [4-8]. Up to now, H₂S corrosion, especially SSC and HIC have attracted considerable attention [9-14]. In the H₂S environment, Fe(II) ions and S²⁻ ion can form non stoichiometric ratio ferrous sulfide compounds [15], and there are different types of crystal structure of the corrosion product film formed on the surface of metal. Shoesmith et al. [16] in Atomic Energy of Canada Limited (AECL) studied corrosion of iron in different PH conditions when in 21 degrees atmospheric pressure, and they obtained the evolution processes of H₂S corrosion products on surface of iron under special conditions. Corrosion environments could lead to different situations of corrosion; many scholars have studied the effects of environmental factors on H₂S corrosion, which are of great guiding significance for our work [17-20]. Among the environmental factors, temperature is an important factor which has great influence on the corrosion behavior of steel in H₂S environment. Some previous works have been performed related to the temperature factor on corrosion of steel, Liu et al. [21] studied the effect of temperature and H₂S concentration on corrosion of X52 pipeline steel, whose corrosion test was carried out in a high temperature and high pressure autoclave. They concluded the major corrosion product evolution and corrosion rate change with the change of temperature and H₂S concentration. Zheng and co-workers [22] investigated the hydrogen permeation behaviors of L360NCS steel under different temperatures in high pressure H₂S environments. Taheri et al. [23] used pipeline steel A516-Gr70 as research material and investigated the effect of temperature on corrosion behavior of steel in sour simulated solution, the results showed that the hydrogen induced cracking can take place in H₂S containing solution. However, previous works about temperature factor were mainly performed in high H₂S pressure environment or they focused on H₂S corrosion in a single temperature, systematically studies about temperature on pipeline steel corrosion in atmospheric pressure wet H₂S environment were few reported.

In this work, the influence of temperature on corrosion behavior of L360NCS pipeline steel and its corrosion products analysis in wet H₂S environments were investigated. As the widely use of electrochemical analysis technology to investigate the corrosion process in recent years [24-26], we also studied the electrochemical behavior of L360NCS steel in wet H₂S environment under different temperatures. Scanning electron microscope (SEM), X-ray diffractometer (XRD) and other means were used to analysis corrosion products.

2. EXPERIMENTAL PROCEDURE

2.1 Materials and sample preparation

Commercial L360NCS pipeline steel was used as the experimental material in this work and its chemical composition (wt%) is shown in table 1. The steel was heated in the temperature range of 920-950 °C and kept for a period of time. Then the material was air cooled to ensure the grain refine and

the uniform distribution of carbide, which led to the elimination of the internal stress of material. The microstructure of the material was those of typical ferrite and pearlite.

Table 1. Chemical composition of L360NCS pipeline steel.

Element	C	Si	Mn	P	S	Cr	Fe
wt.%	0.13	0.4	1.5	0.02	0.003	0.3	Balance

Standard corrosion specimens (50 mm × 10 mm × 3 mm) were used for the corrosion tests and circular specimens with a diameter of 10 mm for the electrochemical measurement. Prior to the tests, all the specimens were ground with silicon carbide paper (grit: 400-1500) until they were smooth enough. Then specimens were rinsed with acetone and ethanol to remove grease and pollutions on the surface of them. Finally, they were dried by hair dryer and were put in a dryer for further testing.

2.2 Corrosion tests

The corrosion tests were performed in 5.0 wt% NaCl solution at atmospheric pressure, temperatures chosen for the tests were 25, 50, 75 and 90 °C, corrosion period was 168 h. Each test use 3 hang-parcel as parallel samples, after 168 h immersion, samples were properly handled and analyzed.

Specimens were hanged in the wide mouth bottle by teflon tape and the bottle was plugged to make sure seal without leakage. Before the corrosion tests, the solution was poured into the bottle to immerse the specimens and deoxygenated. The four bottles hanged with specimens were put in constant-temperature water bath with temperatures of 25, 50, 75 and 90 °C, respectively. Then the solution was saturated with H₂S at a rate of at least 100 ml/min and H₂S was allowed to bubble through the solution.

2.3 Weight loss tests

Weight loss tests were performed following the ASTM G31 standard [27]. Before the corrosion tests, specimens were weighed for three times by digital balance with a precision of 0.0001 g. After the corrosion tests, specimens were taken out and cleaned by distilled water and acetone, then they were dried and stored. Afterwards, the corrosion films on the surface of specimens were removed according to the chemical products-clean up method [28]. After being dried, specimens were weighed again. Corrosion rate was calculated according to the formula:

$$R = \frac{8.76 \times 10^4 \times (M_1 - M_2)}{S \times D} \quad (1)$$

Where R was the corrosion rate, mm/year; M₁ was the sample weight before experiment, g; M₂ was the sample weight after the corrosion products were removed, g; S was the surface area of sample, cm²; D was the density of sample, g/cm³; t was experiment time, h.

2.4 Electrochemical measurements

Electrochemical tests were performed with GAMRY600 Electrochemical Testing System. EIS and polarization curve experiments were conducted utilizing a conventional three-electrode cell system. Circular specimen was used as the working electrode while a sintered graphite rod and an Ag/AgCl electrode were acted as auxiliary electrode and reference electrode, respectively. H₂S-saturated aqueous brine solution with 5.0 wt% NaCl in distilled water was used as the test solution. The test solution was first purged of air with nitrogen for about 1 h. Then the solution was put in the constant-temperature water bath with set temperature. In the meanwhile, the solution was saturated with H₂S at a rate of at least 100 ml/min for approximately 1 h.

EIS measurements were performed with 5 mV sinusoidal perturbation at open circuit potential with frequencies ranging from 10⁵ Hz to 10⁻² Hz. Besides, the polarization curve test was conducted at a scanning rate of 1 mV/s, and a potential interval of $E_{\text{corr}} \pm 300$ mV. All the electrochemical measurements were repeated three times in order to obtain accurate experimental results.

2.5 Analyses of corrosion product films

The crystal structures of the products were investigated by a Bruker AXS XRD-D8 Focus X-ray diffractometer (XRD) equipped with graphite monochromatized CuK α radiation ($\lambda = 0.15406$ nm). The measurement was within the 2 θ range from 10° to 90° with a scanning step of 2 °/min. The surface appearance of corrosion product films was analyzed utilizing SEM-energy-dispersive X-ray spectroscopy (SEM-EDS) micrographs. The micrographs were collected with an FEI Quanta 200F scanning electron microscope.

3. RESULTS AND DISCUSSION

3.1 Characteristics of corrosion products at different temperatures

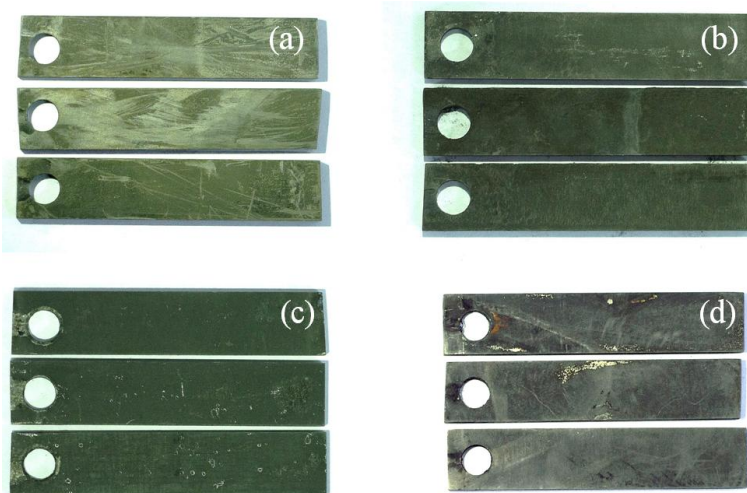


Figure 1. The macro morphology of samples after corrosion at different temperatures. (a) 25 °C, (b) 50 °C, (c) 75 °C, (d) 90 °C.

Fig. 1 shows the macro morphology of the samples after corrosion for 168 h under atmospheric pressure at different temperatures. As shown in the image, as the temperature increased from 25 to 75 °C, the color of the surface of samples darkened. However, when the temperature increased to 90 °C, the color turned shallower, indicating the lower degree of corrosion.

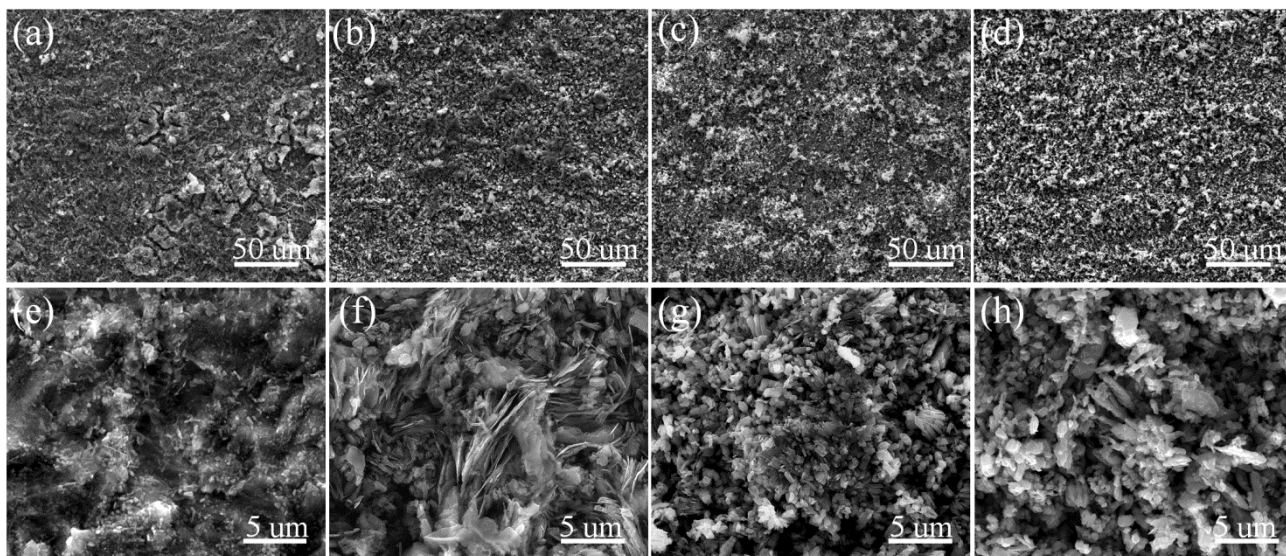


Figure 2. SEM images of samples after corrosion at different temperatures. (a, e) 25 °C, (b, f) 50 °C, (c, g) 75 °C, (d, h) 90 °C.

Fig. 2 shows the SEM images of the samples after corrosion at different temperatures, where Fig. 2e, f, g, h were the moderately magnified images corresponded to Fig. 2a, b, c, d, respectively. It can be seen that the grain size of the corrosion products on the surface of samples turned finer with the increase of temperature.

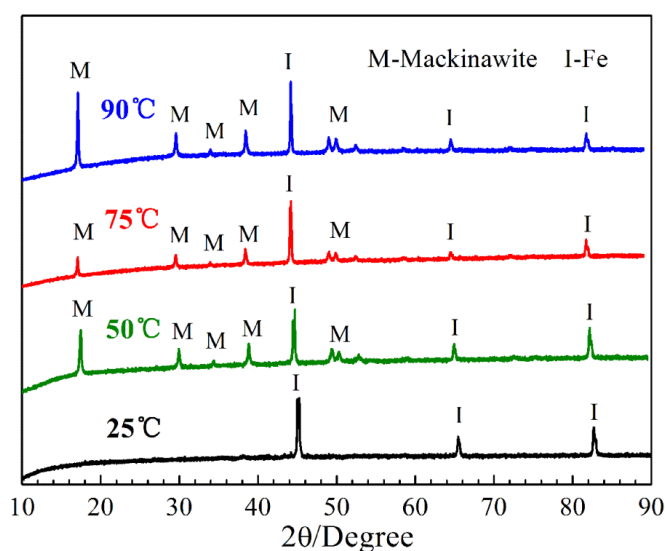


Figure 3. XRD patterns of samples after corrosion at different temperatures.

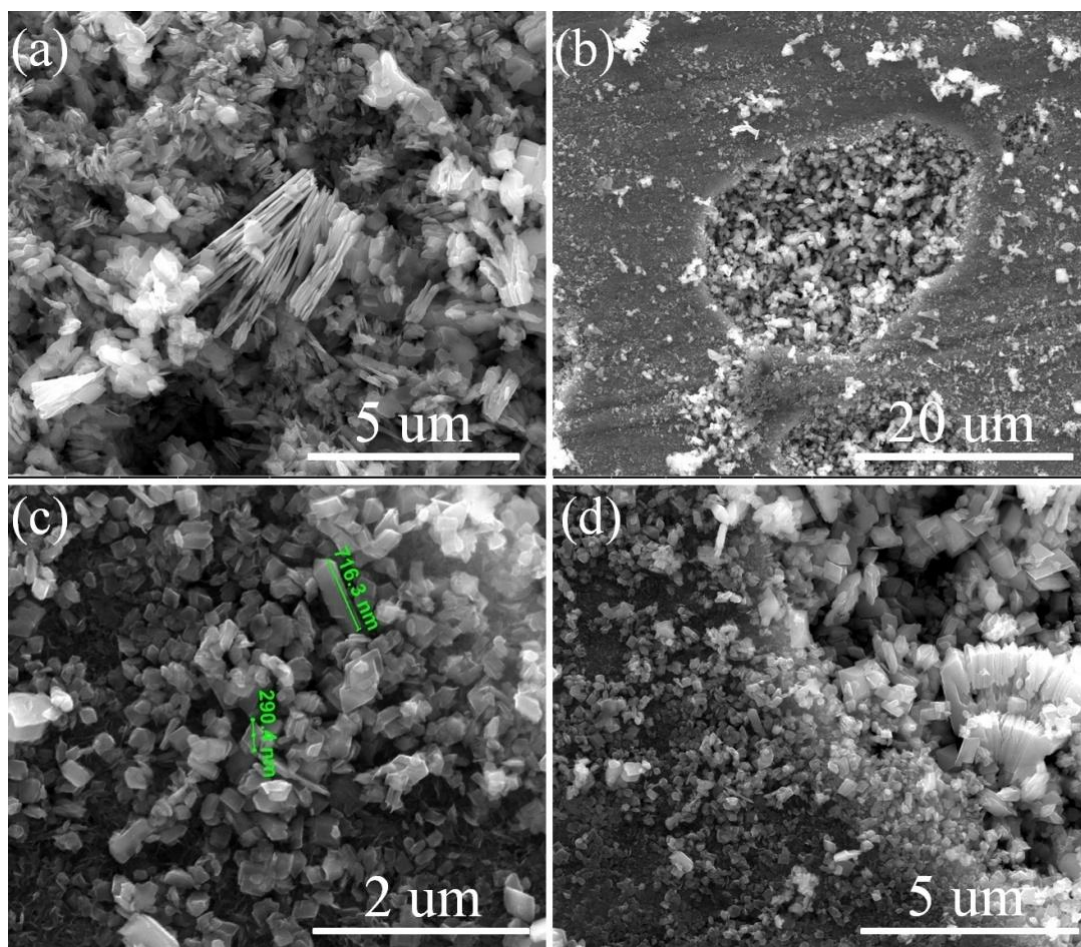


Figure 4. SEM images of samples after corrosion at 75 °C.

The corresponding XRD patterns of the samples after corrosion under different temperatures were shown in Fig. 3. In this test condition, the majority of the corrosion products of the low alloy steel in wet H₂S environment were flake shape mackinawite [29], in the meanwhile, there existed a small amount of amorphous iron sulfide. It was found that the ratio of mackinawite increased as the temperature increased from 25 to 90 °C.

It was obviously observed the rupture of corrosion product films when at the temperature of 75 °C under atmospheric pressure, as presented in Fig. 4. What's more, this rupture phenomenon also happened in other temperature conditions, which indicated that the corrosion products were not continually growing after generated. The occurrence of rupture of corrosion products could be explained according to the previous study. At the beginning a sulfide film was generated rapidly, then, ions in the solution passed through the film and contact with substrate, after which the ions reacted in the interface and generated new corrosion products. The growing corrosion products resulted in the rupture and fallen off of the original sulfide film, finally new corrosion products were covered on the substrate [30].

3.2 Corrosion rate of L360NCS steel

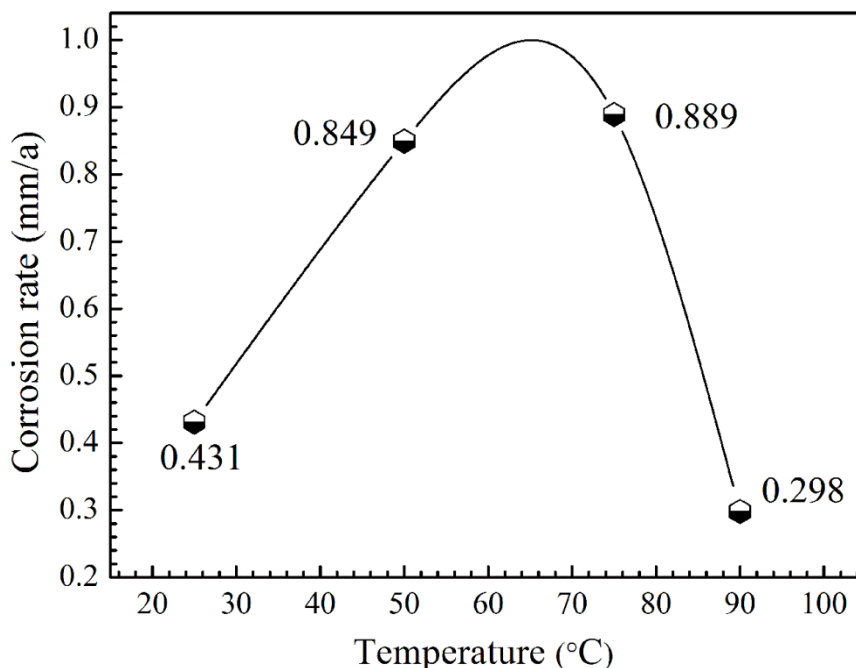


Figure 5. Corrosion rate of L360NCS steel after immersion at different temperatures.

Weight loss method may be the most reliable method to obtain accurate corrosion rate of the samples [31]. Fig. 5 shows the corrosion rates of L360NCS steel in 5.0 wt% NaCl solution at atmospheric pressure H₂S environment under different temperatures. The results were average values. As shown in the image, the corrosion rate increased significantly as temperature increased from 25 to 75 °C, soon afterwards it decreased rapidly with further increase of temperature, and the corrosion rate of 90 °C was even lower than that of 25 °C. This phenomenon may be related to the reduced solubility of H₂S in water. The solubility of H₂S in water decrease clearly with the increase of temperature, for instance, at 25 °C, it is 3.375 g/L, at 50 °C, it is 1.883 g/L, when the temperature increase to 90 °C, the solubility decrease to 0.410 g/L. According to the literature [32], we calculated the concentration of H₂S in test solution at different temperatures, as presented in Table 2.

Table 2. The calculated concentration of H₂S in test solution at different temperatures.

Temperature (°C)	25	50	75	90
C _{H₂S} (mol/L)	0.0967	0.0578	0.0416	0.0361

It can be seen that C_{H₂S} showed a decreasing trend as temperature increased, which was consistent with solubility of H₂S. The structures of the corrosion products formed on steel immersed in solution containing H₂S depended on the temperature and the solubility of H₂S [33-35], then the corrosion products could promote or inhibit the corrosion. In addition, the decrease of solubility of H₂S in water may further led to the changes of solution pH and other conditions, which finally resulted in

the huge decrease of corrosion rate.

3.3 Electrochemical measurements analysis

3.3.1 EIS analysis

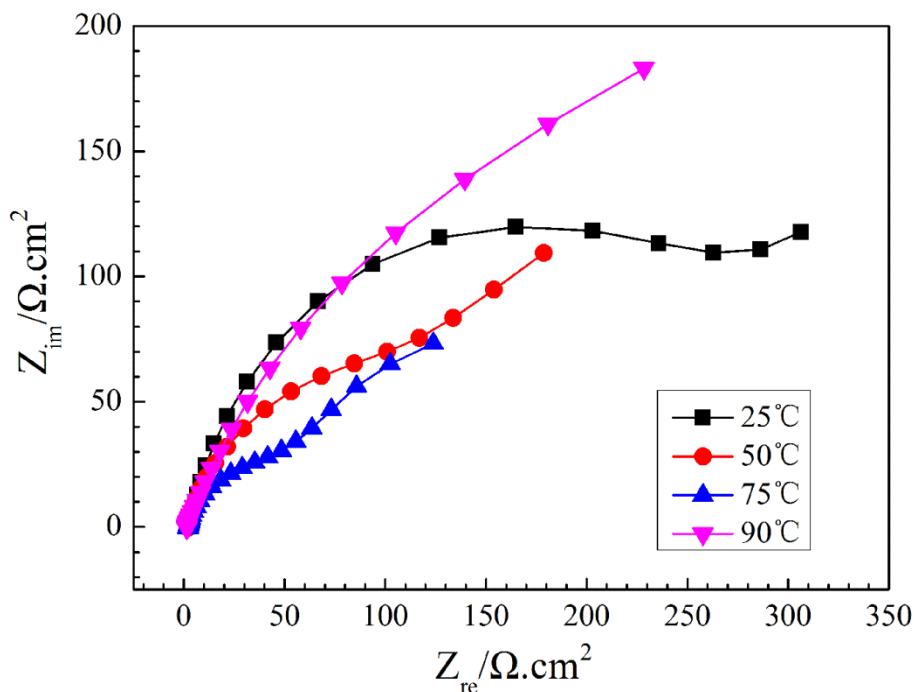


Figure 6. Nyquist impedance diagrams of L360NCS electrode after immersion in H₂S-saturated aqueous brine solution at different temperatures.

Fig. 6 shows the Nyquist impedance diagrams of L360NCS electrode after immersion in H₂S-saturated aqueous brine solution at different temperatures. As presented in the image, when the temperature ranged from 25 to 75 °C, the reaction showed semicircle characteristic at medium-high frequencies and a slope at low frequencies, indicating a charge-transfer and diffusion-controlled mechanism reaction, which was similar to the research result of K. Indira[36]. While at 90 °C, only a semicircle characteristic was observed, which revealed the disappearance of diffusion-controlled behavior, the result represented a charge-transfer reaction. The reason for this occurrence maybe in this temperature, the diffusion rates of ions in the solution were quick enough, which could satisfy for the electrochemical reaction. In the reactions of 25 to 75 °C, there existed a capacitive reactance arc at the high-frequency region and an inflection point at the transition region, indicating Warburg impedance existed in the process of the reaction. At the high-frequency region, concentration polarization of the diffusion-controlled behavior could be ignored [37, 38], the capacitive reactance arc corresponded to the electric double layer behavior. It can be seen that as the temperature increased from 25 to 75 °C, polarization resistance of the reaction gradually reduced, while it changed at the temperature range from 75 to 90 °C. At the low-frequency region, the Nyquist impedance diagram displayed a linear

correlation between real component and virtual component, which indicated the electrode reaction in low-frequency region was mainly diffusion-controlled.

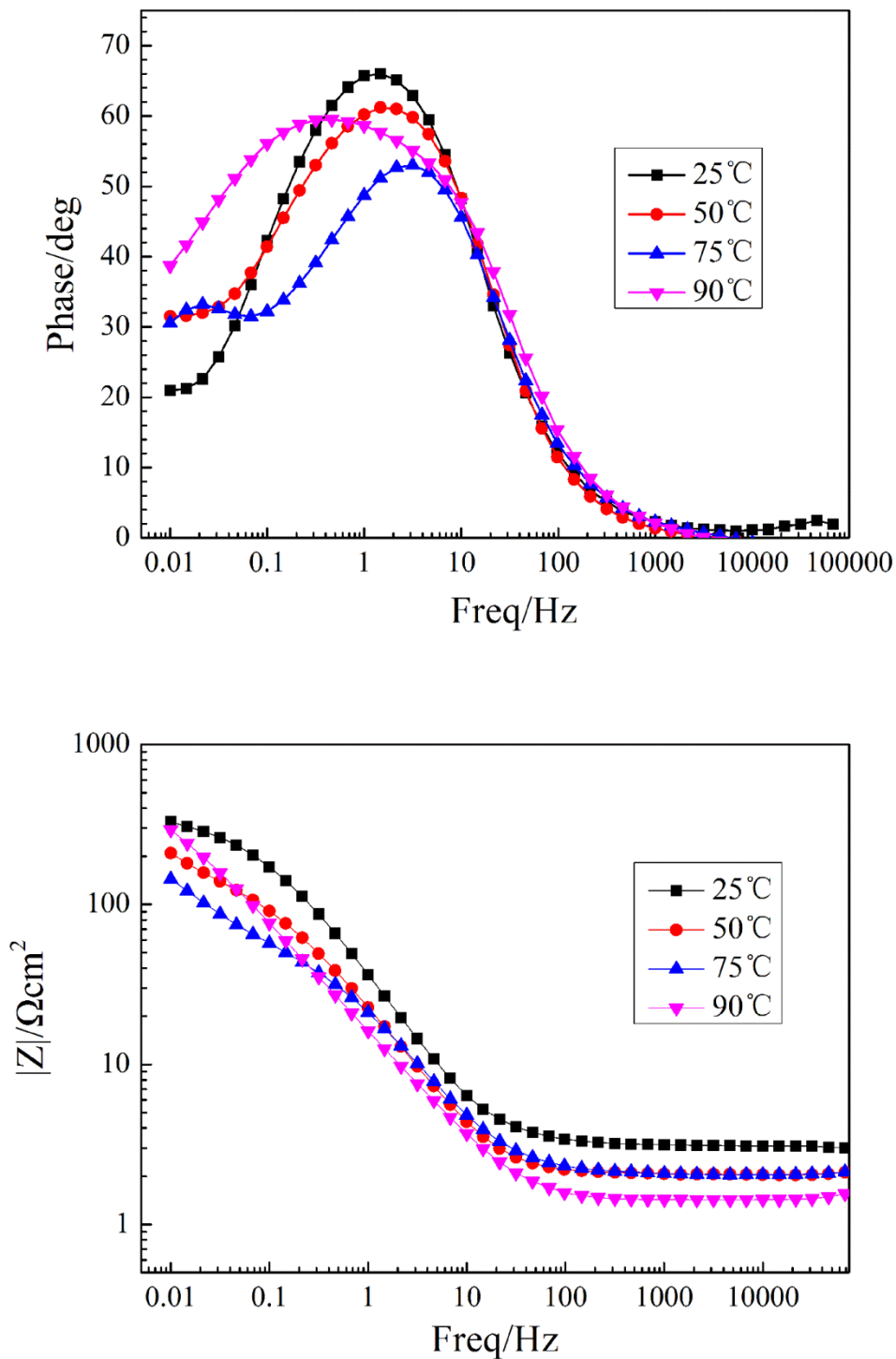


Figure 7. Bode diagrams of L360NCS electrode after immersion in H₂S-saturated aqueous brine solution at different temperatures.

The Bode diagrams of L360NCS steel after immersion at different temperatures are given in Fig. 7. It can be seen that the diagrams showed two time constants at the frequency of approximately 1-10 Hz, while there were certain differences among the corresponding phase angles and frequencies. When temperature increased from 25 to 75 °C, the corresponding phase angles reduced obviously, meanwhile the corresponding frequencies increased slightly, which indicated the corrosion tendency of L360NCS steel was growing with the increase of temperature. When the temperature was 90 °C, the corresponding phase angle was similar to that of 50 °C, which was far larger than that of 75 °C. However, the corresponding frequency of 90 °C was far lower than those of 50 °C and 75 °C, indicating the corrosion tendency of L360NCS at 90 °C was smaller than those of 50 °C and 75 °C. The electrochemical impedance ($|Z|$) and frequency plot showed the $|Z|$ decreased with the increase of temperature at low-frequency region, while the $|Z|$ of 90 °C showed some increase. It has been reported that the surface gets more protected when shows higher $|Z|$ values, particularly at the low frequency region[39], and this agreed with our results too. Additionally, at high-frequency region, the $|Z|$ was nearly unaffected with the variation of frequency.

The electrochemical equivalent circuit for EIS fitting is shown in Fig.8.

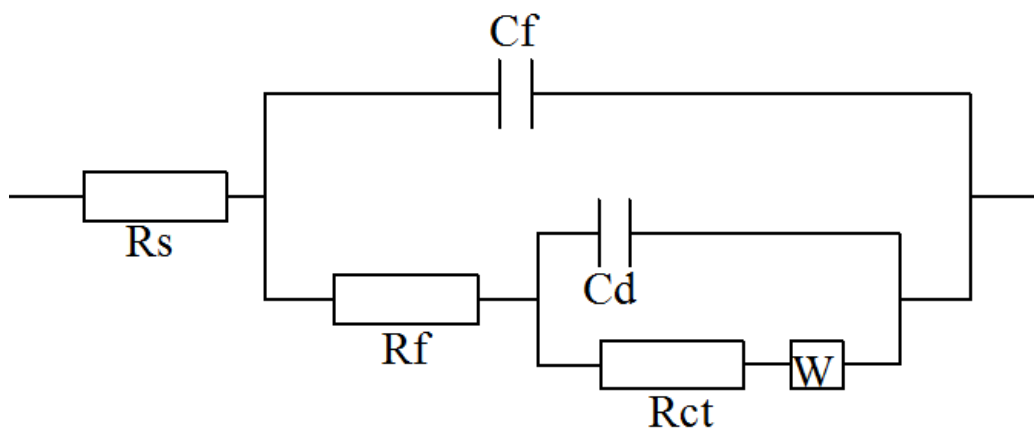


Figure 8. Electrochemical equivalent circuit for EIS fitting.

Commercial software ZSimpWin was applied to conduct the equivalent circuit analysis. In the circuit, R_s was the solution resistance, R_f was the corrosion product film resistance, C_f was the electrical capacity of the corrosion product films, C_d was the electrical double-layer capacitor, R_{ct} was the charge transfer resistance and W was the Warburg impedance. There was no Warburg impedance at 90 °C due to the disappearance of diffusion-controlled behavior.

Table 3. Values of the electrochemical equivalent circuit elements.

T (°C)	R_s ($\Omega \text{ cm}^2$)	C_f (F cm^2)	R_f ($\Omega \text{ cm}^2$)	C_d (F cm^2)	R_{ct} ($\Omega \text{ cm}^2$)	W ($\Omega \text{ cm}^2$)
25	3.614	0.002568	35.86	0.2293	194.1	0.02194
50	2.394	0.003726	1.957	0.0039	67.94	0.02246
75	2.400	0.002655	7.230	0.3078	27.13	0.02988
90	1.727	0.004834	26.27	0.0145	31.68	0

Table 3 shows the values of the electrochemical equivalent circuit elements for each data. It can be seen that at 25 and 90 °C, the values of R_f were far larger than those of 50 and 75 °C, this result was correspond to the corrosion rate, which indicated the corrosion production films of 25 and 90 °C were thicker than the films of 50 and 75 °C, thus, the corrosion resistance were stronger. The value of R_{ct} decreased from 194.1 to 31.68 $\Omega \text{ cm}^2$ with the increase of temperature, this result was attributed to the increasing migration rates of ions in the solution as the temperature increased. The slightly change of value of W was related to the generation and diffusion of corrosion product films as the change of temperature.

3.3.2 Polarization curve analysis

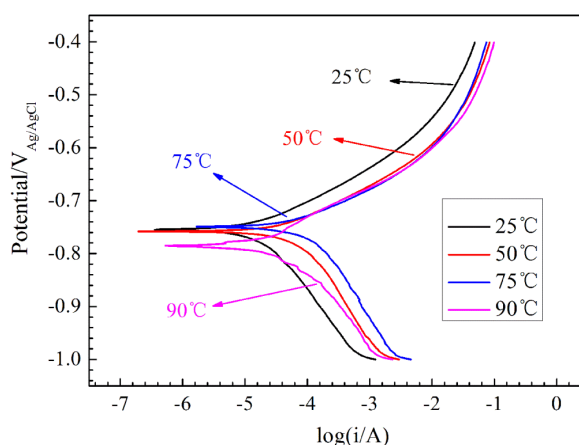


Figure 9. Polarization curve of L360NCS electrode after immersion in H₂S-saturated aqueous brine solution at different temperatures.

The polarization curve of L360NCS steel in H₂S-saturated aqueous brine solution after immersion at 25, 50, 75 and 90 °C is shown in Fig. 9. Polarization curve tests were conducted at a scanning rate of 1 mV/s. It can be seen that with the increase of temperature, the corrosion potential showed a decreasing trend. The electrochemical corrosion parameters e.g. corrosion potential (E_{corr}), cathodic and anodic Tafel slopes (β_a , β_c), corrosion current density (I_{corr}) and linear polarization resistance (LPR) obtained by extrapolation of the Tafel lines are shown in Table 4.

Table 4. Electrochemical parameters obtained from the anodic and cathodic polarization of L360NCS in H₂S-saturated aqueous brine solution after immersion at different temperatures.

T (°C)	$-E_{corr}$ (mV(Ag/AgCl))	I_{corr} (μAcm^{-2})	β_a (mV/dec ⁻¹)	β_c (mV/dec ⁻¹)	LPR (Ωcm^2)	CR (mm/year)
25	0.755	16.09	152.49	71.86	1205	0.1651
50	0.758	58.02	156.79	58.22	348.5	0.5953
75	0.749	94.24	145.82	57.64	226.8	0.8582
90	0.785	17.48	186.95	78.63	937.0	0.1794

It can be seen that the value of I_{corr} increased from 16.09 to 94.24 $\mu\text{A cm}^{-2}$ as the temperature increased from 25 to 75 °C, yet it decreased rapidly to 17.48 $\mu\text{A cm}^{-2}$ at 90 °C. The corrosion rate of L360NCS electrode almost displayed a linear increase process from 25 to 75 °C, just as the results of Burkan Isgor[40], which showed that corrosion rates increased 6-8 folds with temperature rising from 10°C to 60°C. However, similar to the variation trend of I_{corr} , when temperature increased to 90 °C, the corrosion rate showed a sharp decrease. The result of other researchers showed the same trend, while the changing point was not the same [19]. Same conclusion could be made from the linear polarization resistances, the value of LPR decreased from 1205 to 226.8 $\Omega \text{ cm}^2$ as temperature increased from 25 to 75 °C, then it increased to 937 $\Omega \text{ cm}^2$ at 90 °C.

4. CONCLUSIONS

In summary, in the condition of atmospheric pressure wet H_2S environment, the corrosion rate of L360NCS pipeline steel increased first and then decreased with the increase of temperature. The corrosion rates were low at 25 and 90 °C; the corrosion rates were low at 50 and 75 °C. Mackinawite was the main corrosion product and the grain size of corrosion products decreased with the increase of temperature.

EIS result showed the reaction was charge-transfer and diffusion-controlled when temperature ranged from 25 to 75 °C, while it showed a charge-transfer reaction at 90 °C. The polarization curve revealed the linear polarization resistance decreased first and then increased as temperature increased. The results show the corrosion of steel at low temperature (25 °C) and high temperature (90 °C) were slighter than medium temperature (50-75 °C), this phenomenon related to the reduced solubility of H_2S in water and enhanced reaction rate with increased temperature.

ACKNOWLEDGEMENTS

This work was financially supported by the Natural Science Foundation of China (No.51171208 and 51271201), the Science Foundation of China University of Petroleum, Beijing (No. LLYJ-2011-41) and the PhD Basic Research Innovation Foundation of China University of Petroleum, Beijing (No. 2462016YXBS06). We would like to thank Yu Ding for assistance in the corrosion exposure tests.

References

1. B. Brown, K.-L.J. Lee, S. Nestic, *Corrosion*, (2003) 16-20.
2. S. Nešić, *Corros. Sci.*, 49 (12) (2007) 4308-4338.
3. F. Huang, X.G. Li, J. Liu, Y.M. Qu, C.W. Du, *Mater. Corros.*, 63 (1) (2012) 59-66.
4. R.D. Kane, M.S. Cayard, *Corrosion*, (1999) 25-30.
5. S. Zheng, C. Li, Y. Qi, L. Chen, C. Chen, *Corros. Sci.*, 67 (2013) 20–31.
6. R. Galvan-Martinez, J. Mendoza-Flores, R. Duran-Romero, J. Genesca, *Mater. Corros.*, 58 (7) (2007) 514–521.
7. J.E.R. Pinto, J.A.C. Ponciano, *Mater. Corros.*, 52 (3) (2001) 201–203.
8. D.W. Shoesmith, P. Taylor, M.G. Bailey, B. Ikeda, *Electrochim. Acta*, 23 (9) (1978) 903-916.
9. T. Taira, K. Tsukada, Y. Kobayashi, H. Inagaki, T. Watanabe, *Corrosion*, 37 (1) (1981) 5-16.
10. T.Y. Jin, Z.Y. Liu, Y.F. Cheng, *Int. J. Hydrogen. Energy*, 35 (5) (2010) 8014-8021.

11. G. Domizzi, G. Anteri, J. Ovejero-García, *Corros. Sci.*, 43 (2) (2001) 325–339.
12. S.N. Smith, M.W. Joosten, *Corrosion*, (2006) 12-16.
13. M.V. Biezma, *Int. J. Hydrogen Energy*, 26 (5) (2001) 515–520.
14. J. Kittel, V. Smanio, M. Fregonese, L. Garnier, X. Lefebvre, *Corros. Sci.*, 52 (4) (2010) 1386-1392.
15. D. Rickard, G. W. Luther, *Chem. Rev.*, 107 (2) (2007) 514-562.
16. D. W. Shoesmith, P. Taylor, M. G. Bailey, D.G. Owen, *J. Electrochem. Soc.*, 127 (5) (1980) 1007-1015.
17. S. Pal, R.N. Ibrahim, *Corros. Sci.*, 53 (8) (2011) 2660-2669.
18. W. Sun, S. Nestic, *Corrosion*, (2007).
19. Y. Qi, H. Luo, S. Zheng, C. Chen, Z. Lv, M. Xiong, *Int. J. Electrochem. Sci.*, 9 (2014) 2101-2112.
20. J. Tang, Y. Shao, T. Zhang, G. Meng, F. Wang, *Corros. Sci.*, 53 (5) (2011) 1715-1723.
21. M. Liu, J. Q. Wang, W. Ke, *Materials Science Forum*, 743/744 (2013) 589-596.
22. S. Zheng, C. Zhou, P. Wang, C. Chen, L. Chen, *Int. J. Electrochem. Sci.*, 8 (2013).
23. H. Taheri, S. Kakooei, M. C. Ismail, A. Dolati, *Caspian J. Appl. Sci. Res.*, 1 (5) (2012) 41-47.
24. J.M. Zhao, H.B. Duan, R.J. Jiang, *Corros. Sci.*, 91 (2015) 108–119.
25. E. Abelev, T.A. Ramanarayanan, S.L. Bernasek, *J. Electrochem. Soc.*, 156 (9) (2009) C331-C339.
26. Z.F. Yin, W.Z. Zhao, Z.Q. Bai, Y.R. Feng, *Electrochim. Acta*, 53 (10) (2008) 3690-3700.
27. ASTM Standard G31, ASTM International.
28. ISO 8407, International Standardization Organization.
29. P. Bai, S. Zheng, H. Zhao, Y. Ding, J. Wu, C. Chen, *Corros. Sci.*, 87 (2014) 397–406.
30. P. Bai, H. Zhao, S. Zheng, C. Chen, *Corros. Sci.*, 93 (2015) 109-119.
31. E. Poorqasemi, O. Abootalebi, M. Peikari, F. Haqdar, *Corros. Sci.*, 51 (5) (2009) 1043-1054.
32. J. Ding, L. Zhang, M. Lu, J. Wang, Z. Wen, W. Hao, *Appl. Surf. Sci.*, 289 (15) (2014) 33-41.
33. J. Tang, Y. Shao, J. Guo, T. Zhang, G. Meng, F. Wang, *Corros. Sci.*, 52 (6) (2010) 2050-2058.
34. S. Fujimoto, H. Tsuchiya, *Corros. Sci.*, 49 (1) (2007) 195-202.
35. J. Ning, Y. Zheng, D. Young, B. Brown, S. Nešić, *Corrosion*, 70 (4) (2013) 375-389.
36. K. Indira and T. Nishimura, *Int. J. Electrochem. Sci.*, 11 (2016) 419-431.
37. J.G. Llongueras, S.A. Peralta, J.M. Flores, R. Duran-Romero, *Corrosion*, (2003).
38. S. Arzola, J. Mendoza-Flores, R. Duran-Romero, J. Genesca, *Corrosion* 62 (5) (2006) 433-443.
39. F. Mansfeld, S. Lin, S. Kim and H. Shih, *Corros. Sci.*, 27 (1987) 997.
40. M. Pour-Ghaz, O. Burkan Isgor, P. Ghods, *Corros. Sci.*, 51 (2009) 415-425.